The Sloan Digital Sky Survey quasar catalog: tenth data release

Isabelle Pâris, Patrick Petitjean, Éric Aubourg, Nicholas P. Ross, Adam D. Myers, Alina Streblyanska, Stephen Bailey, Patrick B. Hall, Michael A. Strauss, Scott F. Anderson, et al.

A&A 563, A54 (2014)
DOI: 10.1051/0004-6361/201322691

Astronomy & Astrophysics

The Sloan Digital Sky Survey quasar catalog: tenth data release⋆

Isabelle Pâris[1], Patrick Petitjean[2], Éric Aubourg[3], Nicholas P. Ross[4], Adam D. Myers[5,6], Alina Streblyanska[7,8], Stephen Bailey[4], Patrick B. Hall[9], Michael A. Strauss[10], Scott F. Anderson[11], Dmitry Bizyaev[12], Arnaud Borde[13], J. Brinkmann[12], Jo Bovy[14,⋆⋆], William N. Brandt[15,16], Howard Brewington[12], Joel R. Brownstein[17], Benjamin A. Cook[10], Garrett Ebelke[12], Xiaohui Fan[18], Nurten Filiz Ak[15,16,19], Hayley Finley[2], Andreu Font-Ribera[4,20], Jian Ge[21], Fred Hamann[21], Shirley Ho[22], Linhua Jiang[18], Karen Kinemuchi[12], Elena Malanushenko[12], Viktor Malanushenko[12], Moses Marchante[12], Ian D. McGreer[18], Richard G. McMahon[23], Jordi Miralda-Escudé[24,25], Demitri Muna[26], Pasquier Noterdaeme[2], Daniel Oravetz[12], Nathalie Palanque-Delabrouille[13], Kaike Pan[12], Ismaël Perez-Fournon[7,8], Matthew Pieri[27], Rogério Riffel[28,29], David J. Schlegel[4], Donald P. Schneider[15,16], Audrey Simmons[12], Matteo Viel[30,31], Benjamin A. Weaver[32], W. Michael Wood-Vasey[33], Christophe Yèche[13], and Donald G. York[34,35]

(Affiliations can be found after the references)

Received 17 September 2013 / Accepted 13 November 2013

ABSTRACT

We present the Data Release 10 Quasar (DR10Q) catalog from the Baryon Oscillation Spectroscopic Survey (BOSS) of the Sloan Digital Sky Survey III. The catalog includes all BOSS objects that were targeted as quasar candidates during the first 2.5 years of the survey and that are confirmed as quasars via visual inspection of the spectra, have luminosities $M_i[z = 2] < -20.5$ (in a ΛCDM cosmology with $H_0 = 70$ km s^{-1} Mpc^{-1}, $\Omega_M = 0.3$, and $\Omega_\Lambda = 0.7$), and either display at least one emission line with a full width at half maximum (FWHM) larger than 500 km s^{-1} or, if not, have interesting/complex absorption features. The catalog also includes known quasars (mostly from SDSS-I and II) that were reobserved by BOSS. The catalog contains 166 583 quasars (74 454 are new discoveries since SDSS-DR9) detected over 6373 deg^2 with robust identification and redshift measured by a combination of principal component eigenspectra. The number of quasars with $z > 2.15$ (117 668) is ∼5 times greater than the number of $z > 2.15$ quasars known prior to BOSS. Redshifts and FWHMs are provided for the strongest emission lines (C IV, C III, Mg II). The catalog identifies 16 461 broad absorption line quasars and gives their characteristics. For each object, the catalog presents five-band (u, g, r, i, z) CCD-based photometry with typical accuracy of 0.03 mag and information on the optical morphology and selection method. The catalog also contains X-ray, ultraviolet, near-infrared, and radio emission properties of the quasars, when available, from other large-area surveys. The calibrated digital spectra cover the wavelength region 3600–10 500 Å at a spectral resolution in the range $1300 < R < 2500$; the spectra can be retrieved from the SDSS Catalog Archive Server. We also provide a supplemental list of an additional 2376 quasars that have been identified among the galaxy targets of the SDSS-III/BOSS.

Key words. catalogs – surveys – quasars: general

1. Introduction

Quasars have become a key ingredient in our understanding of cosmology and galaxy evolution ever since their discovery (Schmidt 1963). With the advent of large and dedicated surveys such as the Sloan Digital Sky Survey (SDSS; York et al. 2000) and the 2dF Quasar Redshift Survey (2QZ; Croom et al. 2001), the number of known quasars has rapidly increased. The first two stages of the SDSS discovered and spectroscopically confirmed more than 105 000 quasars (Schneider et al. 2010), mainly at low redshift ($z \leq 2$). The Baryonic Oscillation Spectroscopic Survey (BOSS; Dawson et al. 2013), the main dark time survey of the third stage of the SDSS (SDSS-III; Eisenstein et al. 2011), aims to measure the expansion rate of the Universe using the clustering of luminous red galaxies at $z \sim 0.7$ (Anderson et al. 2012) and the clustering of the intergalactic medium (IGM) at $z \sim 2.5$ (Busca et al. 2013; Slosar et al. 2013). To make such a measurement, the BOSS quasar target selection (Ross et al. 2012) is designed to reach a sky density of $z \geq 2.15$ quasars of at least 15 deg^{-2}. The first two years of observation of SDSS-III/BOSS were released as part of the ninth data release (Ahn et al. 2012) whose associated quasar catalog (DR9Q; Pâris et al. 2012) contained 87 822 unique quasars, 61 931 having $z > 2.15$, over an area of 3275 deg^2.

This paper presents the SDSS-DR10 quasar catalog, denoted DR10Q, which compiles all the spectroscopically-confirmed quasars identified during the first three years of BOSS operations and released as part of the SDSS tenth data release (Ahn et al. 2013). This catalog contains quasars targeted by the main quasar target selection (Ross et al. 2012), the BOSS ancillary programs (Dawson et al. 2013) and serendipitous discoveries in the galaxy targets. It contains 166 583 unique quasars, including 117 668 with $z > 2.15$, over an area of 6373 deg^2. In this paper, we summarize the procedures used to compile DR10Q and describe the changes relative to DR9Q (Pâris et al. 2012).

In Sect. 2, we summarize the target selection and observations. We describe the construction of the DR10Q catalog in Sect. 3. We summarize the general properties of the present

⋆ Quasar catalog is only available at the CDS via anonymous ftp to cdsarc.u-strasbg.fr (130.79.128.5) or via http://cdsarc.u-strasbg.fr/viz-bin/qcat?J/A+A/563/A54

⋆⋆ Hubble fellow.

sample in Sect. 4 and describe its detailed contents in Sect. 5. We conclude in Sect. 6. In addition, we explain the programs used to target quasars (main selection and ancillary programs) in Appendix A and the format of the file containing the results of the visual inspection of spectra used to derive the DR10Q catalog in Appendix B. This information is made available on the SDSS public website[1].

In the following, we use a ΛCDM cosmology with $H_0 = 70$ km s^{-1}, $\Omega_M = 0.3$, $\Omega_\Lambda = 0.7$ (Spergel et al. 2003). We call a quasar an object with a luminosity $M_i[z = 2] < -20.5$ that either displays at least one emission line with *FWHM* > 500 km s^{-1} or, if not, has specific absorption features that can be securely identified as quasars due to the Lyman-α forest or BAL troughs. This definition is the same as in DR9Q (Pâris et al. 2012). In the following, all magnitudes are PSF magnitudes (Stoughton et al. 2002) and are corrected for Galactic extinction using the maps from Schlegel et al. (1998).

2. Observations

A surface density of ∼15 quasars per deg^2 in the redshift range 2.15−3.5 is necessary to measure the BAO scale in the Lyman-α forest at $z \sim 2.5$ (McDonald & Eisenstein 2007). SDSS-III/BOSS is a five-year program that aims at observing over 160 000 $z > 2.15$ quasars over 10 000 deg^2 in order to reach a precision of 4.5% on the angular diameter distance and 2.6% on the Hubble constant at $z \sim 2.5$ (Eisenstein et al. 2011). The first detection of the baryon acoustic oscillation (BAO) signal in the clustering of the IGM was obtained from the spectra of the ∼60 000 high redshift quasars listed in the DR9Q catalog (Busca et al. 2013; Slosar et al. 2013).

2.1. Imaging data

Quasar target selection for BOSS is based on imaging released in SDSS-DR8 (Aihara et al. 2011); it is the same as in SDSS-I/II with an extension to the South Galactic Cap (SGC). These data were gathered using a dedicated 2.5 m wide-field telescope (Gunn et al. 2006) to collect light for a camera with 30 $2k \times 2k$ CCDs (Gunn et al. 1998) over five broad bands – *ugriz* (Fukugita et al. 1996); this camera has imaged 14 555 unique square degrees of the sky, including contiguous areas of ∼7500 deg^2 in the North Galactic Cap (NGC) and ∼3100 deg^2 in the SGC that comprise the uniform "Legacy" areas of the SDSS (Aihara et al. 2011). The imaging data were acquired on dark photometric nights of good seeing (Hogg et al. 2001). Objects were detected and their properties were measured (Lupton et al. 2001; Stoughton et al. 2002) and calibrated photometrically (Smith et al. 2002; Ivezić et al. 2004; Tucker et al. 2006; Padmanabhan et al. 2008), and astrometrically (Pier et al. 2003). The BOSS limiting magnitude for target selection is $r \leq 21.85$ or $g \leq 22$.

2.2. Target selection

The measurement of clustering of the IGM is independent of the properties of background quasars, but does depend on the surface density of quasar lines of sight. Hence, the target selection for the quasars used for Lyman-α forest cosmology does not have to be uniform, but should maximize the surface density of high-z quasars. However, there is also the desire to perform demographic measurements using a uniformly-selected quasar sample. Thus, a [composite] strategy that mixes a heterogeneous selection to maximize the surface density of $z > 2.15$ quasars, with a uniform subsample has been adopted by SDSS-III/BOSS (Ross et al. 2012).

On average, 40 fibers per deg^2 are allocated to the quasar project. Approximately half of these are selected through the target selection algorithm intended to create a uniform ("CORE") sample. After testing during the first year of BOSS observations, the CORE selection was chosen to be the XDQSO method (Bovy et al. 2011) The other half of the fibers are dedicated to quasar candidates that are used to maximize the surface density [at the cost of homogeneity] of high-redshift quasars: the "BONUS" sample. Several different methods (a neural network combinator: Yèche et al. (2010); a Kernel Density Estimator, KDE: Richards et al. (2004, 2009); a likelihood method: Kirkpatrick et al. (2011), and the XDQSO method with lower likelihood than in the CORE sample) were implemented to select the BONUS quasar targets. Where available, near-infrared data from UKIDSS (Lawrence et al. 2007), ultraviolet data from GALEX (Martin et al. 2005), along with deeper coadded imaging in overlapping SDSS runs (Aihara et al. 2011), were also incorporated to increase the high-z quasar yield (Bovy et al. 2012). Point sources that match the FIRST radio survey (July 2008 version; Becker et al. 1995) with $(u - g) > 0.4$ (to filter out $z < 2.15$ quasars) are always included in the quasar target selection.

Previously known quasars were also re-targeted[2] to take advantage of the improved throughput of the SDSS spectrographs. The sample of previously known quasars were drawn from multiple sources. These include: SDSS-DR7 quasar catalog (Schneider et al. 2010); the 2dF QSO redshift survey (2QZ; Croom et al. 2004); the 2dF-SDSS LRG and QSO survey (2SLAQ; Croom et al. 2009); the AAT-UKIDSS-DSS (AUS) survey, and the MMT-BOSS pilot survey (Appendix C in Ross et al. 2012). Quasars observed at high spectral resolution by VLT/UVES and Keck/Hires were also included in the sample.

In addition to the main survey, about 5% of the SDSS-III/BOSS fibers are allocated to ancillary programs. They are described in the Appendix and Tables 6 and 7 of Dawson et al. (2013) and Sect. 4.2 of Ahn et al. (2013). The full list of ancillary programs (and their target selection bits) that target quasars and thus, are included in the present catalog, is provided in Appendix A.

2.3. Spectroscopy

Quasar targets selected by the various target selection algorithms are spectroscopically observed with the BOSS spectrographs whose spectral resolution varies from ∼1300 at 3600 Å to 2500 at 10 000 Å (Smee et al. 2013). Spectroscopic observations are taken in a series of at least three 15-min exposures. Additional exposures are taken until the squared signal-to-noise ratio per pixel, $(S/N)^2$, reaches the survey-quality threshold for each CCD. These thresholds are $(S/N)^2 \geq 22$ at i-band magnitude 21 for the red camera and $(S/N)^2 \geq 10$ at g-band magnitude 22 for the blue camera (Galactic extinction-corrected magnitudes). The spectroscopic reduction pipeline for BOSS spectra is described in Bolton et al. (2012). SDSS-III uses plates with 1000 spectra each, which can overlap (Dawson et al. 2013). A total of 1515 plates were observed between December 2009 and July 2012, some plates were observed multiple times. In total, 166 583 unique quasars have been spectroscopically confirmed

[1] http://www.sdss3.org/dr10/algorithms/qso_catalog.php

[2] During the first two years of observations, we re-targeted only $z > 2.15$ known quasars. We have extended the re-observation to known $z > 1.8$ quasars since Year 3.

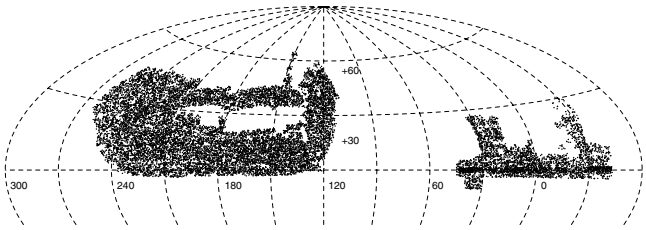

Fig. 1. Distribution on the sky of the SDSS-DR10/BOSS spectroscopy in J2000 equatorial coordinates. Note that the RA = 0 point is offset from the center.

based on our visual inspection as we describe below. Figure 1 shows the observed sky area. The total area covered by the SDSS-DR10 is 6373 deg^2.

3. Construction of the DR10Q catalog

The SDSS-DR10 quasar catalog is built upon the visual inspection of the spectra of all the objects targeted as quasars by SDSS-III/BOSS and all the objects classified robustly as $z \geq 2$ quasars by the SDSS pipeline (Bolton et al. 2012) among the galaxy targets.

3.1. Visual inspection process

The visual inspection process is fully described in Sect. 3 of Pâris et al. (2012); we briefly summarize the steps here.

The spectra of quasar candidates are reduced and the SDSS pipeline[3] provides a classification (`QSO`, `STAR` or `GALAXY`) and a redshift. Each spectrum is fit with a library of star templates, a PCA decomposition of galaxy spectra and a PCA decomposition of quasar spectra. Each class of templates is fit over a range of redshifts: galaxies from $z = -0.01$ to 1.00, quasars from $z = 0.0033$ to 7.00, and stars from $z = -0.004$ to 0.004 (± 1200 km s^{-1}). The combination of redshift and template with the overall best fit (in terms of the lowest reduced chi-squared) is adopted as the pipeline classification and redshift measurement. The redshift is accompanied by a flag (`ZWARNING`); when it is zero, the pipeline has high confidence in its estimate. We use this output as a first estimate for the visual inspection.

Through a dedicated website, quasar candidates are separated between low-z quasars ($z < 2$), high-z quasars ($z \geq 2$), stars and "others" based on the initial SDSS pipeline classification. The spectra of the objects in each list are then visually inspected and each object is classified as `QSO`, `Star`, `Galaxy` if the identification and the redshift are certain, `QSO_Z?` if the object is clearly a quasar but the redshift is uncertain, `QSO_?` and `Star_?` if we have clues to the correct classification but are not certain, `?` if we cannot certify the classification of an object at all and `Bad` when the signal-to-noise ratio is too low to identify the objects. The distinction between `?` and `Bad` becomes quite subjective as the signal-to-noise ratio decreases.

In addition to the quasar candidates, we also visually inspected the spectra of some objects among the galaxy targets. While confirming the identification of all the quasar targets is important for understanding and improving the various quasar target selection algorithms, objects are inspected among the galaxy targets to get back the maximum number of serendipitous quasars in the full SDSS-III/BOSS spectroscopic sample.

[3] The software used is called idlspec2d and is publicly available. The current version is v5_5_12. Details can be found at `http://www.sdss3.org/dr10/software` and in Bolton et al. (2012).

Table 1. Number of objects identified as such by the pipeline with any `ZWARNING` value (second column) and with `ZWARNING` = 0 (third column), and after the visual inspection (fourth column).

Classification	# pipeline	# pipeline with `ZWARNING` = 0	# visual inspection
`QSO`	188 705	162 857	166 583
`QSO` with $z > 2.15$	(124 062)	(115 429)	(117 668)
`QSO_?`	–	–	1370
`QSO_Z?`	–	–	545
`Galaxy`	20 627	14 512	10 267
`Star`	112 397	83 429	133 557
`Star_?`	–	–	1519
`Bad`	–	–	3257
`?`	–	–	1082
Missing[a]	–	–	150
Not a quasar (galaxy targets)	–	–	3398
Total	321 729	260 798	321 729

Notes. [(a)] Quasars not visually inspected because of bad photometric information.

Moreover, these objects usually have low signal-to-noise ratio, and thus, their identification is more difficult. For these reasons, the visual inspection strategy is slightly different for this class of objects, and we adopted a binary classification: either an object is a `QSO` or this is *not a quasar*.

3.2. Definition of the DR10Q parent sample

We selected quasar candidates among the objects targeted by the main quasar target selection (labelled as `BOSS_TARGET1` in the SDSS database, Ross et al. 2012), the ancillary programs that target quasars (`ANCILLARY_TARGET1` and `ANCILLARY_TARGET2`, see the Appendix of Dawson et al. 2013) and objects identified as `QSO` with $z > 2$ and `ZWARNING` = 0 by the SDSS pipeline or identified as `GALAXY` with the subclass `BROADLINE`. This leads to a superset of 316 947 quasar targets (i.e. objects targeted for spectroscopy as quasars) and 4782 possible serendipitous quasars from the galaxy targets for a total number of objects of 321 729. The spectra of 321 579 of these have been visually inspected, and 150 quasar targets are missing because of bad photometric information. 166 583 objects have been identified as `QSO`, 545 as `QSO_Z?`, 1370 as `QSO_?`, 10 267 as `Galaxy`, 133 557 as `Star`, 1519 as `Star_?`, 1082 as `?` and 3257 as `Bad`. The result of the visual inspection is given in Table 1.

This quasar catalog lists all the firmly confirmed quasars (`QSO` and `QSO_BAL`, i.e. `QSO` showing broad absorption lines, only). About 10% of these quasars have been observed spectroscopically several times (Dawson et al. 2013). These repeat observations are often useful to confirm the nature of objects with low S/N spectra. However, we did not attempt to co-add these data mostly because they are often of quite different S/N.

Together with the quasar catalog, we provide the full result of the visual inspection (e.g. the identification of all visually scanned objects) with the whole superset from which we derived this catalog. We encode the identification using two parameters `z_conf_person` and `class_person`. The relation between these two parameters and the output from the visual inspection is given in Table 2. We refer the reader to Appendix B to find the detailed format of the fits file that contains the DR10Q superset.

Finally, in the course of various tests for the inclusion of galaxy targets in the visual inspection process, we gathered a

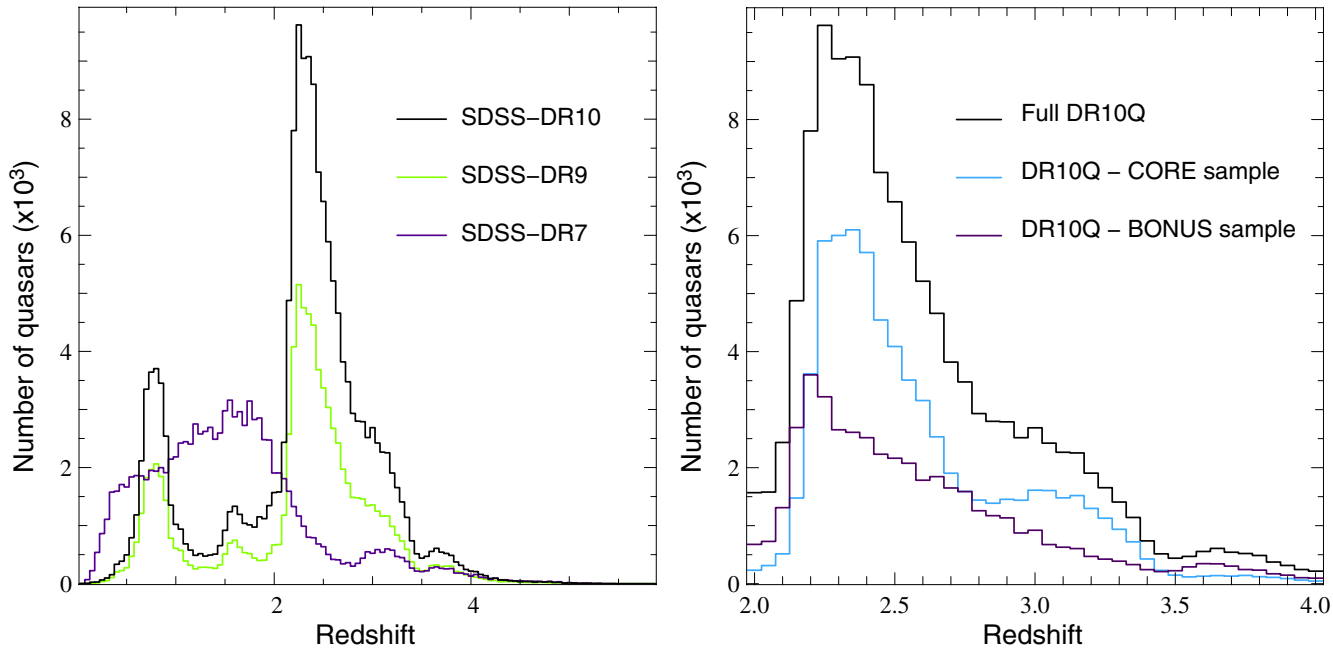

Fig. 2. *Left panel*: redshift distribution of the SDSS-DR10 (black histogram), SDSS-DR9 (green histogram; Pâris et al. 2012) and SDSS-DR7 (purple histogram; Schneider et al. 2010) quasars over the redshift range 0−6. *Right panel*: redshift distribution of the full SDSS-DR10 quasar sample (black histogram), and the SDSS-DR10 CORE (blue histogram) and BONUS (purple histogram) samples over the redshift range 2 to 4. Note that the full DR10Q sample includes CORE, BONUS and quasars observed as part of ancillary programs.

Table 2. Visual inspection classification, corresponding to the combination of the `class_person` (first column) and `z_conf_person` (first row) values provided in the superset file described in Appendix B.

	z_conf_person			
	0	1	2	3
class_person				
0	Not inspected	?	–	–
1	–	–	Star_?	Star
2	Not a quasar[a]	–	–	–
3	–	QSO_?	QSO_Z?	QSO
4	–	–	–	Galaxy
30	–	–	–	QSO_BAL

Notes. [(a)] Galaxy targets.

sample of serendipitous quasars. The parent sample of these objects is not well defined as the visual inspection strategy for the galaxy targets has changed several times. Hence, we provide them in the form of a supplementary list that contains 2376 quasars.

4. Summary of sample

4.1. Broad view

The DR10Q catalog contains 166 583 unique quasars, including 117 668 with $z > 2.15$. This sample contains about twice as many quasars as the previous release (DR9Q). The first 2.5 years of operations of SDSS-III/BOSS cover an area of 6373 deg^2, leading to a mean density of 16.3 $z > 2.15$ quasars per square degree.

The quasars from this catalog have redshifts between 0.053 and 5.855. Their redshift distribution is shown in Fig. 2 (left panel). The peaks at $z \sim 0.8$ and $z \sim 1.6$ are due to known degeneracies in the SDSS color space. The SDSS-DR9 (green histogram) and SDSS-DR10 (black histogram) redshift distributions are scaled versions of one another. The right panel of Fig. 2 displays the same distribution but in the redshift range of interest for BOSS ($2.00 \leq z \leq 4.00$) together with the distributions from the CORE (uniformly selected sample; blue histogram) and the BONUS (purple histogram) samples. Typical spectra of SDSS-DR10 quasars are shown in Fig. 3. The broad statistical properties of this sample have not changed since DR9Q. We list below the differences between the two catalogs, and refer the reader to Pâris et al. (2012) for a detailed description of the unchanged content.

4.2. Differences between SDSS-DR9 and SDSS-DR10 quasar catalogs

4.2.1. Quasars that were in DR9Q but not in DR10Q and quasars that could have been in DR9Q but were not

The DR9Q catalog (Pâris et al. 2012) contained 87 822 unique quasars of which 86 952 are also part of the present catalog. Two plates (3698 and 5369) were accidentally included in DR9 (Ahn et al. 2012), although they did not fulfill the minimum S/N conditions (see Dawson et al. 2013). They have been downgraded to "bad plates", and therefore not included in DR10 (Ahn et al. 2013). These plates have been redrilled, and reobserved after the DR10 cut-off. Hence, 90 DR9 quasars have dropped out of the present catalog. The remaining 786 quasars that were part of DR9Q but not DR10Q were re-classified during various tests of the visual inspection process and are now part of the supplementary list as explained in Sect. 3.

In addition, the identification of 56 objects have changed between DR9Q and DR10Q. This modification is due to systematic checks performed in the past year on objects classified as `QSO_?` and `?`. These checks are necessary especially since objects can be reobserved, often with better S/N and the data reduction pipeline

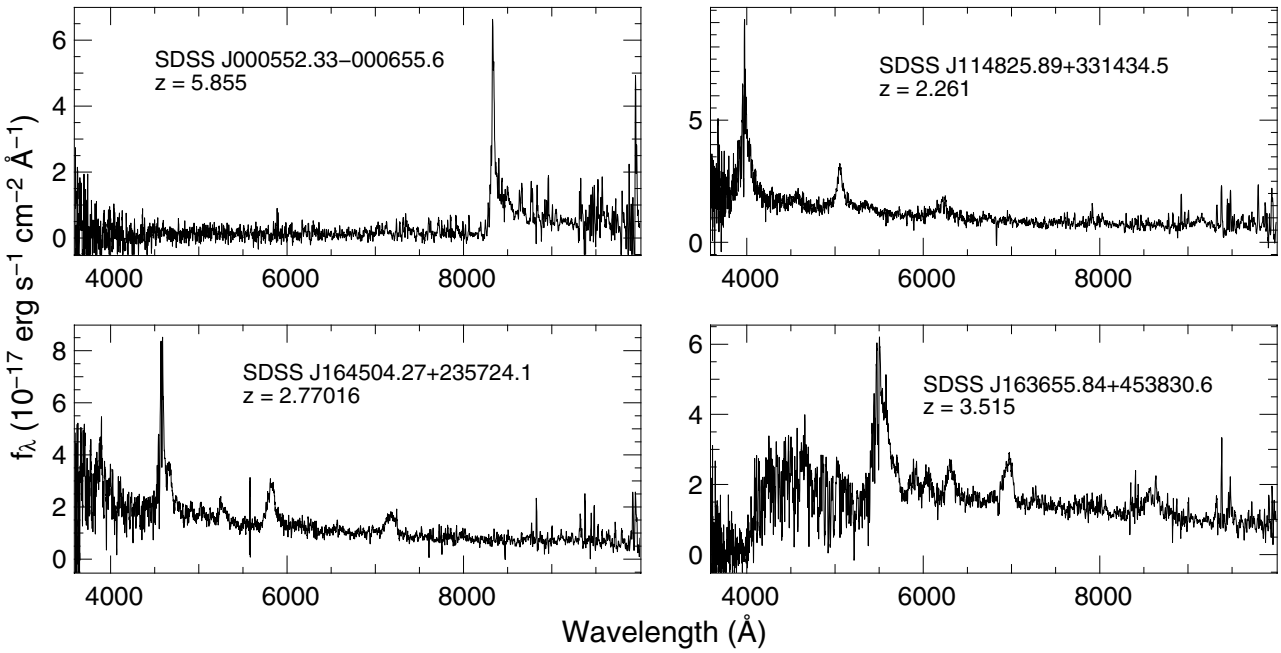

Fig. 3. Highest redshift quasar of the SDSS-DR10 quasar catalog is shown in the *upper left panel*. Note that this quasar was already in DR9Q. The three other panels show typical examples of quasar spectra at different redshift.

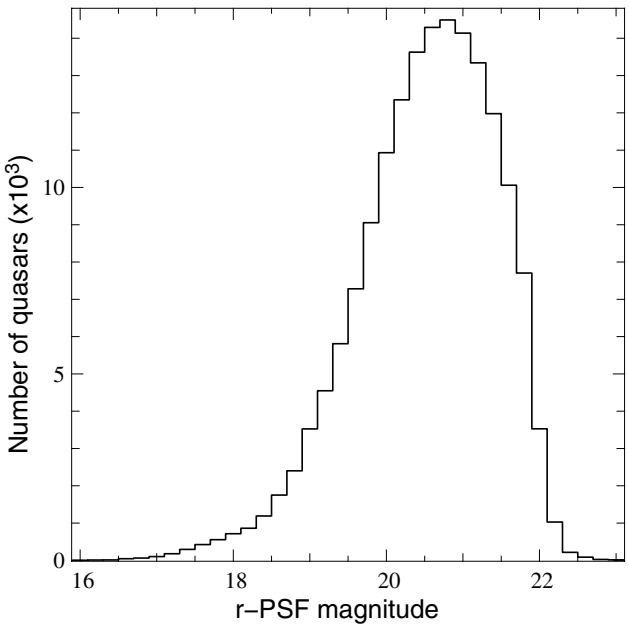

Fig. 4. Distribution of *r*-PSF magnitude (corrected for Galactic extinction) of the quasars included in the DR10Q catalog.

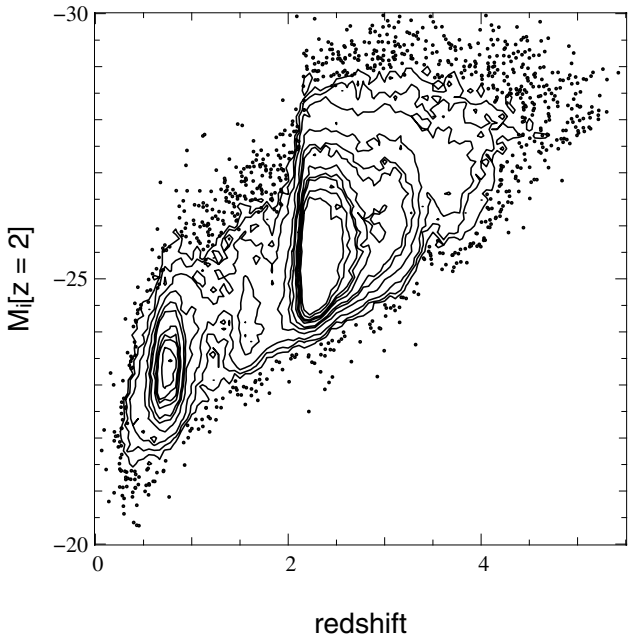

Fig. 5. Luminosity-redshift plane for DR10Q quasars (black contours and points). The luminosity assumes $H_0 = 70$ km s^{-1} Mpc^{-1} and the *k*-correction is given by Richards et al. (2006) who consider $K(z = 2) = 0$. Contours are drawn at constant point density.

constantly improves. We perform this re-inspection after the release of a new data reduction. A few mistakes have also been corrected, after feedback from users of the catalog.

4.2.2. Visual inspection redshift

As part of the visual inspection, we use the SDSS pipeline redshift estimate (`Z_PIPE`) as a first guess, and we either confirm or correct for it when it is necessary. We use the maximum of the Mg II emission line, when it is available in the spectrum, to set the visual inspection redshift (`Z_VI`). Figure 6 shows the distribution of velocity differences between the pipeline and the visual inspection redshift estimates.

In the course of the checks mentioned above, some redshifts have been adjusted. In addition, in the DR9Q catalog (Pâris et al. 2012), the visual inspection redshifts have a 3 digit precision because it is not possible to reach higher precision by eye. The pipeline redshift estimate has a 5 digit precision. In DR9Q, the truncation of the visual redshift was performed even when the visual inspection simply confirmed the pipeline redshift. This approach created a systematic and arbitrary mean

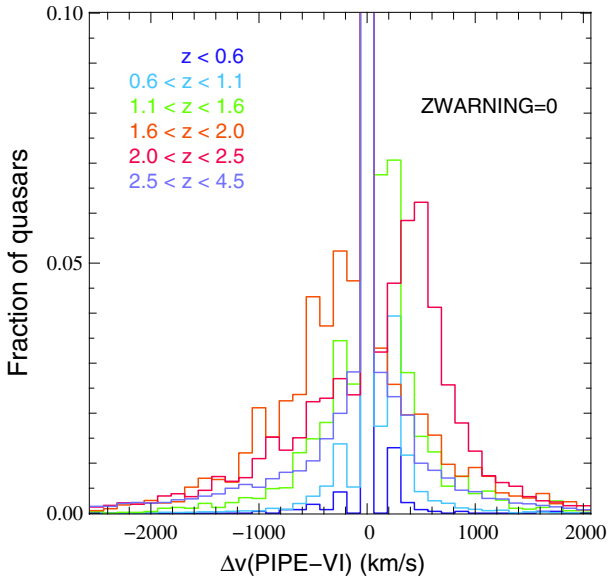

Fig. 6. Distribution of velocity differences between the pipeline and the visual inspection redshift estimates in different bins of redshift. Depending on the redshift bin, the fraction of redshift that we correct increases up to ∼50%.

blueshift of 50 km s^{-1} of the visual redshift estimate relative to the pipeline estimate. In DR10Q we do not apply this truncation.

4.2.3. Emission line fitting

We fit several emission lines (C IV, the C III] complex and Mg II) using a set of principal components. This fit provides a measurement of the line redshift, FWHM, blue and red HWHMs and their equivalent width. We apply the exact same procedure as in DR9Q (see Sect. 4 of Pâris et al. 2012).

However, the set of principal components used in DR9Q was unable to reproduce emission lines with FWHM smaller than 2000 km s^{-1} (Alexandroff et al. 2013), creating an arbitrary truncation of FWHM at this value. We corrected for this defect by incorporating quasars with C IV emission lines of FWHM smaller than 2000 km s^{-1} in the sample used to derive the set of principal components. This modification does not affect most of the measured emission line properties with a median difference for the measured C IV FWHM of ∼50 km s^{-1} between DR9Q and DR10Q. This change does not affect the quality of the PCA redshift estimate neither. Over the $0.6 \leq z \leq 2.3$ sample, where the Mg II emission line is available in the SDSS-III/BOSS spectra, the median shift between the global PCA redshift estimate (`Z_PCA`) and the Mg II redshift is less than 5 km s^{-1}.

4.3. Uniform sample

As in DR9Q, we provide a `uniform` flag (row #26 of Table 3) in order to identify a homogeneously selected sample of quasars. Although the CORE sample has been designed to have a well understood, uniform, and reproducible selection function, its definition has varied over the first year of the survey. Thus, the nominal CORE quasars are not a uniformly-selected sample. Areas within which all the algorithms used in the quasar target selection are uniform are called "Chunks". The definition of each of them can be found in Ross et al. (2012). After Chunk 12, CORE targets were selected with the XDQSO technique alone (Bovy et al. 2011). These objects have `uniform` = 1. Quasars in our catalog with `uniform` = 2 are objects that would have been selected by XDQSO if it had been the CORE algorithm prior to Chunk 12. Objects with `uniform` = 2 are reasonably complete to what XDQSO would have selected, even prior to Chunk 12. But, as DR10Q only contains information about spectroscopically confirmed quasars, not about all *targets*, care must be taken to create a statistical sample from the uniform flag. See, e.g., the discussion regarding the creation of a statistical sample for clustering measurements in White et al. (2012). Quasars with `uniform` = 0 are not homogeneously selected CORE targets.

4.4. Broad absorption line quasars

Broad absorption lines, BALs, in quasar spectra are both visually and automatically identified and characterized as described in Sect. 5 of Pâris et al. (2012).

In total we identified 16 461 BAL quasars during the visual inspection of the DR10 quasar candidates. The visual inspection does not measure the width of troughs, but C IV troughs are also automatically identified and characterized in the spectra of $z \geq 1.57$ quasars. This redshift is chosen so that the whole region between Si IV and C IV emission lines is covered by the BOSS spectrograph.

We provide the balnicity index (BI; Weymann et al. 1991) and the absorption index (AI; Hall et al. 2002) for these quasars. A total of 9623 quasars with `Z_VI` ≥ 1.57 have a positive BI value and 26 232 have AI > 0 km s^{-1}. The systematic search is performed for C IV troughs *only*: some quasars flagged BAL by the visual inspection may have BI = 0 km s^{-1}, either because the condition that troughs must be at least 2000 km s^{-1} wide is not fullfilled, or because the object was flagged because of absorption lines of some other ion (e.g. Mg II, Si IV). The distribution of the two indices is shown in Fig. 7.

4.5. Multiwavelength matching

We cross-correlate the DR10Q catalog with several other surveys: the FIRST radio survey (Becker et al. 1995), the Galaxy Evolution Explorer (GALEX, Martin et al. 2005) survey in the UV, the Two Micron All Sky Survey (2MASS, Cutri et al. 2003; Skrutskie et al. 2006), the Wide-Field Infrared Survey (WISE, Wright et al. 2010) and the ROSAT All-Sky Survey (RASS, Voges et al. 1999, 2000). In addition, we now provide a match to the UKIRT Infrared Deep Sky Survey (UKIDSS, Lawrence et al. 2007) and the second *XMM-Newton* serendipitous source catalog (Watson et al. 2009).

4.5.1. FIRST

We match the DR10Q catalog to the FIRST radio survey (Becker et al. 1995) using a 2″matching radius as we did in DR9Q. We use the FIRST catalog released in February 2012, which contains an extension in the SGC which is not included in the July 2008 catalog that was used to match to DR9Q quasars. We report the flux peak density at 20 cm and the signal-to-noise ratio of the detection. If a quasar lies outside of the FIRST footprint, the reported flux density peak is set to −1.

The SDSS-III/BOSS quasar target selection (Ross et al. 2012) automatically includes the FIRST sources from the *previous* (July 2008) version of the FIRST catalog with $(u - g) > 0.4$. This additional color cut is set to avoid contamination by low-redshift quasars.

There are 6682 matches to the FIRST catalog.

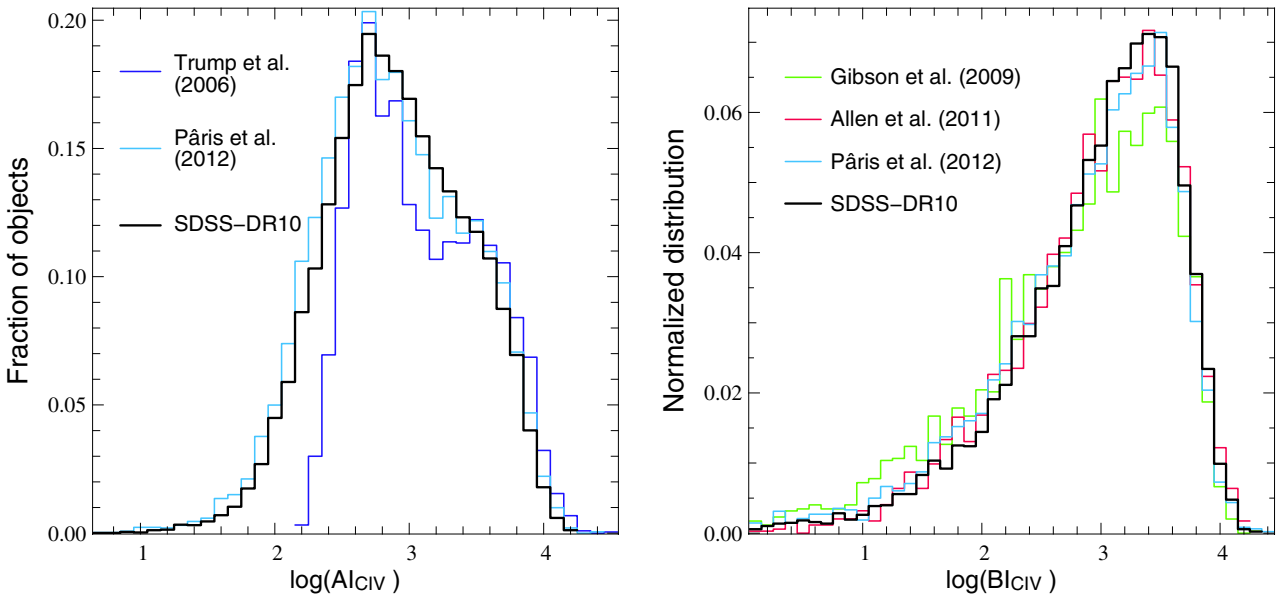

Fig. 7. *Left panel*: distribution of AI measured for C IV absorption troughs from Trump et al. (2006, blue histogram), SDSS-DR9 (cyan histogram, Pâris et al. 2012) and the present catalog (thick black histogram). The distributions are normalized for log AI > 3. *Right panel*: distribution of BI measured for the C IV absorption troughs from Gibson et al. (2009, green histogram), Allen et al. (2011, red histogram), SDSS-DR9 (cyan histogram, Pâris et al. 2012), and the present catalog (thick black histogram).

4.5.2. The Galaxy Evolution Explorer (GALEX)

As in DR9Q, GALEX (Martin et al. 2005) images are force photometered (from GALEX Data Release 5) at the SDSS-DR8 centroids (Aihara et al. 2011), such that low S/N point-spread function fluxes of objects not detected by GALEX is obtained, for both the FUV (1350−1750 Å) and NUV (1750−2750 Å) bands when available.

A total of 107 835 quasars are detected in the NUV band, 86 753 in the FUV band and 69 164 have non-zero fluxes in both bands.

4.5.3. The Two Micron All Sky Survey (2MASS)

We cross-correlate the DR10Q catalog with the All-Sky Data Release Point Source catalog (Skrutskie et al. 2006) using a matching radius of 2″. We report the Vega-based magnitudes in the J, H and K-bands and their error together with the signal-to-noise ratio of the detections. We also provide the value of the 2MASS flag rd_flg[1], which gives the meaning of the peculiar values of the magnitude and its error for each band[4].

There are 2824 matches in the catalog.

4.5.4. The Wide-Field Infrared Survey (WISE)

As we did for DR9Q, we match the BOSS DR10Q to the WISE All-Sky Source Catalog[5] (Wright et al. 2010). Our procedure is the same as in DR9Q, with a matching radius of 2.0″providing a very low-level of false positive matches (see e.g. Fig. 4 of Krawczyk et al. 2013). We find 87 849 matches from the WISE All-Sky Source Catalog.

Here, we report the magnitudes, their associated errors, the S/N of the detection and reduced χ^2 of the profile-fitting in the four WISE bands centered at wavelengths of 3.4, 4.6, 12 and 22 μm. These magnitudes are in the Vega system, and are measured with profile-fitting photometry[6].

However, we *strongly caution* the reader not to accept our catalog matches in blind faith. We report the WISE catalog Contamination and confusion flag, `cc_flags`, and as suggested on the WISE "Cautionary Notes" page[7] recommend using only those matches with `cc_flags` = "0000" to exclude objects which are flagged as spurious detections of image artifacts in any band. However, our checks have found that even this criterion sometimes selects catalog objects that are obviously spurious in the WISE imaging.

4.5.5. UKIDSS

The UKIRT Infrared Deep Sky Survey (UKIDSS, Lawrence et al. 2007) has observed 7500 deg^2 in the near infrared. UKIDSS images are force photometered at the SDSS-DR8 centroids (Aihara et al. 2011). UKIDSS observations acquired before March 2011 were used; they have been released as UKIDSS DR1-DR9.

We provide the fluxes and their associated errors, expressed in W m^{-2} Hz^{-1}, in the Y, J, H and K bands. The conversion to the Vega magnitudes, used in 2MASS, is given by the formula:

$$\mathrm{mag_X} = -2.5 \times \log \frac{f_\mathrm{X}}{f_{0,\mathrm{X}} \times 10^{-26}}, \quad (1)$$

where X denotes the filter and the zero-point values $f_{0,\mathrm{X}}$ are 2026, 1530, 1019 and 631 for the Y, J, H and K bands respectively.

A total of 66 649 quasars are detected in one of the four bands Y, J, H or K. 65 997 objects are detected in the Y band,

[4] see http://www.ipac.caltech.edu/2mass/releases/allsky/doc/explsup.html for more details.

[5] http://irsa.ipac.caltech.edu/Missions/wise.html

[6] see e.g. http://wise2.ipac.caltech.edu/docs/release/allsky/expsup/sec2_2a.html and http://wise2.ipac.caltech.edu/docs/release/allsky/expsup/sec4_4c.html#wpro

[7] http://wise2.ipac.caltech.edu/docs/release/allsky/expsup/sec1_4b.html#unreliab

65 732 in the J band, 65 730 in H band, 66 130 in the K band and 64 181 objects have non-zero fluxes in the four bands. The UKIDSS limiting magnitude is $K \sim 18$ (for the Large Area Survey) while the 2MASS limiting magnitude in the same band is ∼15.3. This difference in depth between the two surveys explains the very different numbers of matches with DR10Q.

4.5.6. ROSAT all sky survey

As in DR9Q, we cross-correlate DR10Q with the ROSAT all sky survey Faint (Voges et al. 2000) and Bright (Voges et al. 1999) source catalogues with a matching radius of 30″. Only the most reliable detections are included in our catalog: when the quality detection is flagged as potentially problematic, we do not include the match.

There are 57 matches with the Bright Source Catalog and 586 with the Faint Source Catalog.

4.5.7. *XMM-Newton*

We cross-correlate the DR10Q catalog with the second *XMM-Newton* Serendipitous Source Catalog (Third Data Release, 2XMMi-DR3; Watson et al. 2009) using a standard 5″ matching radius. The 2XMMi-DR3 catalog has observed 512 deg^2, with possible multiple observations of a given sky area.

We report the soft (0.5–2 keV) and hard (2–10 keV) fluxes, expressed in erg cm^{-2} s^{-1} and the corresponding X-ray luminosities, expressed in erg s^{-1}. The latter are computed from the flux in each band using the visual inspection redshift (`Z_VI`) and $H_0 = 70$ km s^{-1} Mpc^{-1}, $\Omega_M = 0.3$, $\Omega_\Lambda = 0.7$.

A total of 506 of the sources have been observed more than once. In these cases, the observation with the longest exposure time has been used to compute the fluxes.

The *XMM-Newton* telescope has a set of three X-ray CCD cameras (MOS1, MOS2 and PN). The European Photon Imaging Camera (EPIC-PN) is preferred because of its higher quantum efficiency. If one source has no PN observation or insufficient amount of counts, the average of MOS1 and MOS2 camera fluxes was used to improve statistics. Reported fluxes for sources with less than 30 counts in each camera are given as the mean of the fluxes in PN, MOS1 and MOS2. Finally, in case of no detection or detection with significant errors (less than 1σ detections), we provide an upper limit for the flux in the hard band (2–10 keV). Such sources have the flag `LX2_10_UPPER` set to −1.

There are 2311 matches with the 2XMMi-DR3 catalog.

5. Description of the DR10Q catalog

The DR10Q catalog is available as a binary FITS table file at the SDSS public website[8]. The FITS header contains all of the required documentation (format, name, unit of each column). Table 3 provides a summary of the information contained in each of the columns in the catalog.

Notes on the catalog columns:

1. The DR10 object designation, given by the format SDSS Jhhmmss.ss+ddmmss.s; only the final 18 characters are listed in the catalog (i.e., the character string "SDSS J" is dropped). The coordinates in the object name follow IAU convention and are truncated, not rounded.

2−3. The J2000 coordinates (Right Ascension and Declination) in decimal degrees. The astrometry is from SDSS-DR10 (see Ahn et al. 2012).

4. The 64-bit integer that uniquely describes the objects that are listed in the SDSS (photometric and spectroscopic) catalogs (`THING_ID`).

5−7. Information about the spectroscopic observation (spectroscopic plate number, modified Julian Date, and spectroscopic fiber number) used to determine the characteristics of the spectrum. These three numbers are unique for each spectrum, and can be used to retrieve the digital spectra from the public SDSS database. When an object has been observed several times, we selected the best quality spectrum as defined by the SDSS pipeline (Bolton et al. 2012), i.e. with `SPECPRIMARY` = 1.

8. Redshift from the visual inspection, `Z_VI`.

9. Redshift from the BOSS pipeline (Bolton et al. 2012).

10. Error on the BOSS pipeline redshift estimate.

11. ZWARNING flag from the pipeline. ZWARNING > 0 indicates uncertain results in the redshift-fitting code (Bolton et al. 2012).

12. Automatic redshift estimate using a linear combination of four principal components (see Sect. 4 of Pâris et al. 2012, for details). When the velocity difference between the automatic PCA and visual inspection redshift estimates is larger than 3000 km s^{-1}, this PCA redshift is set to −1.

13. Error on the automatic PCA redshift estimate. If the PCA redshift is set to −1, the associated error is also set to −1.

14. Estimator of the PCA continuum quality (between 0 and 1) as given in Eq. (11) of Pâris et al. (2011).

15−17. Redshifts measured from the C IV, the C III] complex and the Mg II emission lines from a linear combination of five principal components (see Pâris et al. 2012). The line redshift is estimated using the maximum of each emission line, contrary to `Z_PCA` (Col. #12) that is a global estimate using all the information available in a given spectrum.

18. Morphological information: objects classified as point source by the SDSS photometric pipeline have `SDSS_MORPHO` = 0 while extended quasars have `SDSS_MORPHO` = 1. The vast majority of the quasars included in the present catalog are unresolved (`SDSS_MORPHO` = 0) as it is a requirement of the main quasar target selection (Ross et al. 2012).

19−21. The main target selection information is tracked with the `BOSS_TARGET1` flag bits (19; see Table 2 in Ross et al. 2012, for a full description). Ancillary program target selection is tracked with the `ANCILLARY_TARGET1` (20) and `ANCILLARY_TARGET2` (21) flag bits. The bit values and the corresponding program names are listed in Dawson et al. (2013) and Appendix B.

22. A quasar previously known from the SDSS-DR7 quasar catalog (Schneider et al. 2010) has an entry equal to 1, and 0 otherwise. During Year 1 and 2, all SDSS-DR7 quasars with $z \geq 2.15$ were reobserved. After Year 2, all SDSS-DR7 quasars with $z \geq 1.8$ have been reobserved.

23−25. Spectroscopic plate number, Modified Julian Date, and spectroscopic fiber number in SDSS-DR7.

26. `Uniform` flag. See Sect. 4.3.

27. Spectral index α_ν. The continuum is approximated by a power-law, $f_{\rm cont} \propto \nu^{\alpha_\nu}$, and is computed in emission line free regions: 1450−1500 Å, 1700−1850 Å and 1950−2750 Å in the quasar rest frame.

28. Median signal-to-noise ratio per pixel computed over the whole spectrum.

[8] http://www.sdss3.org/dr10/algorithms/qso_catalog.php

Table 3. DR10Q catalog format.

Column	Name	Format	Description[a]
1	SDSS_NAME	STRING	SDSS-DR10 designation hhmmss.ss+ddmmss.s (J2000)
2	RA	DOUBLE	Right Ascension in decimal degrees (J2000)
3	DEC	DOUBLE	Declination in decimal degrees (J2000)
4	THING_ID	INT32	Thing_ID
5	PLATE	INT32	Spectroscopic Plate number
6	MJD	INT32	Spectroscopic MJD
7	FIBERID	INT32	Spectroscopic Fiber number
8	Z_VI	DOUBLE	Redshift from visual inspection
9	Z_PIPE	DOUBLE	Redshift from BOSS pipeline
10	ERR_ZPIPE	DOUBLE	Error on BOSS pipeline redshift
11	ZWARNING	INT32	ZWARNING flag
12	Z_PCA	DOUBLE	Refined PCA redshift
13	ERR_ZPCA	DOUBLE	Error on refined PCA redshift
14	PCA_QUAL	DOUBLE	Estimator of the PCA continuum quality
15	Z_CIV	DOUBLE	Redshift of C IV emission line
16	Z_CIII	DOUBLE	Redshift of C III] emission complex
17	Z_MGII	DOUBLE	Redshift of Mg II emission line
18	SDSS_MORPHO	INT32	SDSS morphology flag 0 = point source 1 = extended
19	BOSS_TARGET1	INT64	BOSS target flag for main survey
20	ANCILLARY_TARGET1	INT64	BOSS target flag for ancillary programs
21	ANCILLARY_TARGET2	INT64	BOSS target flag for ancillary programs
22	SDSS_DR7	INT32	1 if the quasar is known from DR7
23	PLATE_DR7	INT32	SDSS-DR7 spectroscopic Plate number if the quasar is known from DR7
24	MJD_DR7	INT32	SDSS-DR7 spectroscopic MJD if the quasar is known from DR7
25	FIBERID_DR7	INT32	SDSS-DR7 spectroscopic Fiber number if the quasar is known from DR7
26	UNIFORM	INT32	Uniform sample flag
27	ALPHA_NU	FLOAT	Spectral index measurement α_ν
28	SNR_SPEC	FLOAT	Median signal-to-noise ratio over the whole spectrum
29	SNR_1700	FLOAT	Median signal-to-noise ratio in the window 1650–1750 Å (rest frame)
30	SNR_3000	FLOAT	Median signal-to-noise ratio in the window 2950–3050 Å (rest frame)
31	SNR_5150	FLOAT	Median signal-to-noise ratio in the window 5100–5250 Å (rest frame)
32	FWHM_CIV	DOUBLE	FWHM of C IV emission line in km s^{-1}
33	BHWHM_CIV	DOUBLE	Blue HWHM of C IV emission line in km s^{-1}
34	RHWHM_CIV	DOUBLE	Red HWHM of C IV emission line in km s^{-1}
35	AMP_CIV	DOUBLE	Amplitude of C IV emission line in units of median rms pixel noise
36	REWE_CIV	DOUBLE	Rest frame equivalent width of C IV emission line in Å
37	ERR_REWE_CIV	DOUBLE	Uncertainty on the rest frame equivalent width of C IV emission line in Å
38	FWHM_CIII	DOUBLE	FWHM of C III] emission complex in km s^{-1}
39	BHWHM_CIII	DOUBLE	Blue HWHM of C III] emission line in km s^{-1}
40	RHWHM_CIII	DOUBLE	Red HWHM of C III] emission line in km s^{-1}
41	AMP_CIII	DOUBLE	Amplitude of C III] emission complex in units of median rms pixel noise
42	REWE_CIII	DOUBLE	Rest frame equivalent width of C III] emission line in Å
43	ERR_REWE_CIII	DOUBLE	Uncertainty on the rest frame equivalent width of C III] emission complex in Å
44	FWHM_MGII	DOUBLE	FWHM of Mg II emission line in km s^{-1}
45	BHWHM_MGII	DOUBLE	Blue HWHM of Mg II emission line in km s^{-1}
46	RHWHM_MGII	DOUBLE	Red HWHM of Mg II emission line in km s^{-1}
47	AMP_MGII	DOUBLE	Amplitude of Mg II emission line in units of median rms pixel noise
48	REWE_MGII	DOUBLE	Rest frame equivalent width of Mg II emission line in Å
49	ERR_REWE_MGII	DOUBLE	Uncertainty on the rest frame equivalent width of Mg II emission in Å
50	BAL_FLAG_VI	INT32	BAL flag from visual inspection
51	BI_CIV	DOUBLE	Balnicity index of C IV trough (in km s^{-1})
52	ERR_BI_CIV	DOUBLE	Error on the Balnicity index of C IV trough (in km s^{-1})
53	AI_CIV	DOUBLE	Absorption index of C IV trough (in km s^{-1})
54	ERR_AI_CIV	DOUBLE	Error on the absorption index of C IV trough (in km s^{-1})
55	CHI2THROUGH	DOUBLE	χ^2 of the trough from Eq. (3) in Pâris et al. (2012)
56	NCIV_2000	INT32	Number of distinct C IV troughs of width larger than 2000 km s^{-1}
57	VMIN_CIV_2000	DOUBLE	Minimum velocity of the C IV troughs defined in row 51 (km s^{-1})
58	VMAX_CIV_2000	DOUBLE	Maximum velocity of the C IV troughs defined in row 51 (in km s^{-1})
59	NCIV_450	INT32	Number of distinct C IV troughs of width larger than 450 km s^{-1}
60	VMIN_CIV_450	DOUBLE	Minimum velocity of the C IV troughs defined in row 53 (in km s^{-1})
61	VMAX_CIV_450	DOUBLE	Maximum velocity of the C IV troughs defined in row 53 (in km s^{-1})

Notes. [(a)] All magnitudes are PSF magnitudes.

Table 3. continued.

Column	Name	Format	Description[a]
62	REW_SIIV	DOUBLE	Rest frame equivalent width of the Si IV trough
63	REW_CIV	DOUBLE	Rest frame equivalent width of the C IV trough
64	REW_ALIII	DOUBLE	Rest frame equivalent width of the Al III trough
65	RUN_NUMBER	INT32	SDSS Imaging Run Number of photometric measurements
66	PHOTO_MJD	INT32	Modified Julian Date of imaging observation
67	RERUN_NUMBER	STRING	SDSS Photometric Processing Rerun Number
68	COL_NUMBER	INT32	SDSS Camera Column Number (1−6)
69	FIELD_NUMBER	INT32	SDSS Field Number
70	OBJ_ID	STRING	SDSS Object Identification Number
71	PSFFLUX	FLOAT[5]	Flux in the u, g, r, i and z-bands (not corrected for Galactic extinction)
72	IVAR_PSFLUX	FLOAT[5]	Inverse variance of u, g, r, i and z fluxes
73	PSFMAG	FLOAT[5]	PSF magnitudes in u, g, r, i and z-bands (not corrected for Galactic extinction)
74	ERR_PSFMAG	FLOAT[5]	Error in u, g, r, i and z PSF magnitudes
75	TARGET_FLUX	FLOAT[5]	TARGET flux in the u, g, r, i and z-bands (not corrected for Galactic extinction)
76	MI	FLOAT	$M_i\,[z=2]\left(H_0 = 67.8\ \mathrm{km\ s^{-1}\ Mpc^{-1}},\ \Omega_M = 0.308,\ \Omega_\Lambda = 0.692,\ \alpha_\nu = -0.5\right)$
77	DGMI	FLOAT	$\Delta(g-i) = (g-i) - \langle(g-i)\rangle_{\mathrm{redshift}}$ (Galactic extinction corrected)
78	GAL_EXT	FLOAT[5]	Galactic extinction in the 5 SDSS bands from Schlegel et al. (1998)
79	GAL_EXT_RECAL	FLOAT[5]	Galactic extinction in the 5 SDSS bands from Schlafly & Finkbeiner (2011)
80	HI_GAL	FLOAT	$\log N_H$ (logarithm of Galactic H I column density in $\mathrm{cm^{-2}}$)
81	RASS_COUNTS	DOUBLE	log RASS full band count rate (counts $\mathrm{s^{-1}}$)
82	RASS_COUNTS_SNR	FLOAT	S/N of the RASS count rate
83	SDSS2ROSAT_SEP	DOUBLE	SDSS-RASS separation in arcsec
84	N_DETECTION_XMM	INT32	Number of detections in *XMM-Newton*
85	FLUX05_2KEV	DOUBLE	Soft (0.5−2 keV) X-ray flux from *XMM-Newton* (erg $\mathrm{cm^{-2}\ s^{-1}}$)
86	FLUX2_12KEV	DOUBLE	Hard (2−12 keV) X-ray flux from *XMM-Newton* (erg $\mathrm{cm^{-2}\ s^{-1}}$)
87	LUM05_2KEV	DOUBLE	Soft (0.5−2 keV) X-ray luminosity from *XMM-Newton* (erg $\mathrm{s^{-1}}$) using Z_VI and $H_0 = 70\ \mathrm{km\ s^{-1}\ Mpc^{-1}},\ \Omega_M = 0.3,\ \Omega_\Lambda = 0.7$
88	LUM2_12KEV	DOUBLE	Hard (2−12 keV) X-ray luminosity from *XMM-Newton* (erg $\mathrm{s^{-1}}$) using Z_VI and $H_0 = 70\ \mathrm{km\ s^{-1}\ Mpc^{-1}},\ \Omega_M = 0.3,\ \Omega_\Lambda = 0.7$
89	LUMX2_10_UPPER	DOUBLE	Flag for upper limit of hard X-ray flux (in Col. #86)
90	SDSS2XMM_SEP	DOUBLE	SDSS-*XMM-Newton* separation in arcsec
91	GALEX_MATCHED	SHORT	GALEX match
92	FUV	DOUBLE	*fuv* flux (GALEX)
93	FUV_IVAR	DOUBLE	Inverse variance of *fuv* flux
94	NUV	DOUBLE	*nuv* flux (GALEX)
95	NUV_IVAR	DOUBLE	Inverse variance of *nuv* flux
96	JMAG	DOUBLE	J magnitude (Vega, 2MASS)
97	ERR_JMAG	DOUBLE	Error in J magnitude
98	JSNR	DOUBLE	J-band S/N
99	JRDFLAG	INT32	J-band photometry flag
100	HMAG	DOUBLE	H magnitude (Vega, 2MASS)
101	ERR_HMAG	DOUBLE	Error in H magnitude
102	HSNR	DOUBLE	H-band S/N
103	HRDFLAG	INT32	H-band photometry flag
104	KMAG	DOUBLE	K magnitude (Vega, 2MASS)
105	ERR_KMAG	DOUBLE	Error in K magnitude
106	KSNR	DOUBLE	K-band S/N
107	KRDFLAG	INT32	K-band photometry flag
108	SDSS2MASS_SEP	DOUBLE	SDSS-2MASS separation in arcsec
109	W1MAG	DOUBLE	$w1$ magnitude (Vega, WISE)
110	ERR_W1MAG	DOUBLE	Error in $w1$ magnitude
111	W1SNR	DOUBLE	S/N in $w1$ band
112	W1CHI2	DOUBLE	χ^2 in $w1$ band
113	W2MAG	DOUBLE	$w2$ magnitude (Vega, WISE)
114	ERR_W2MAG	DOUBLE	Error in $w2$ magnitude
115	W2SNR	DOUBLE	S/N in $w2$ band
116	W2CHI2	DOUBLE	χ^2 in $w2$ band
117	W3MAG	DOUBLE	$w3$ magnitude (Vega, WISE)
118	ERR_W3MAG	DOUBLE	Error in $w3$ magnitude
119	W3SNR	DOUBLE	S/N in $w3$ band
120	W3CHI2	DOUBLE	χ^2 in $w3$ band
121	W4MAG	DOUBLE	$w4$ magnitude (Vega, WISE)
122	ERR_W4MAG	DOUBLE	Error in $w4$ magnitude
123	W4SNR	DOUBLE	S/N in $w4$ band
124	W4CHI2	DOUBLE	χ^2 in $w4$ band

Table 3. continued.

Column	Name	Format	Description[a]
125	CC_FLAGS	STRING	WISE contamination and confusion flag
126	SDSS2WISE_SEP	DOUBLE	SDSS-WISE separation in arcsec
127	UKIDSS_MATCHED	SHORT	UKIDSS Matched
128	YFLUX	DOUBLE	Y-band flux from UKIDSS (in W m^{-2} Hz^{-1})
129	YFLUX_ERR	DOUBLE	Error in Y-band flux from UKIDSS (in W m^{-2} Hz^{-1})
130	JFLUX	DOUBLE	J-band flux from UKIDSS (in W m^{-2} Hz^{-1})
131	JFLUX_ERR	DOUBLE	Error in J-band flux from UKIDSS (in W m^{-2} Hz^{-1})
132	HFLUX	DOUBLE	H-band flux from UKIDSS (in W m^{-2} Hz^{-1})
133	HFLUX_ERR	DOUBLE	Error in H-band flux from UKIDSS (in W m^{-2} Hz^{-1})
134	KFLUX	DOUBLE	K-band flux from UKIDSS (in W m^{-2} Hz^{-1})
135	KFLUX_ERR	DOUBLE	Error in K-band flux from UKIDSS (in W m^{-2} Hz^{-1})
136	FIRST_MATCHED	INT	FIRST matched
137	FIRST_FLUX	DOUBLE	FIRST peak flux density at 20 cm expressed in mJy
138	FIRST_SNR	DOUBLE	S/N of the FIRST flux density
139	SDSS2FIRST_SEP	DOUBLE	SDSS-FIRST separation in arcsec

29−31. Median signal-to-noise ratio per pixel computed over the windows 1650−1750 Å (29), 2950−3050 Å (30), 2950−3050 Å (31) in the quasar rest frame. If the wavelength range is not covered by the BOSS spectrum, the value is set to −1.

32−35. FWHM (km s^{-1}), blue and red half widths at half-maximum (HWHM; the sum of the latter two equals FWHM), and amplitude (in units of the median rms pixel noise, see Sect. 4 of Pâris et al. 2012) of the C IV emission line. If the emission line is not in the spectrum, the red and blue HWHM and the FWHM are set to −1.

36−37. Rest frame equivalent width and corresponding uncertainty in Å of the C IV emission line. If the emission line is not in the spectrum, these quantities are set to −1.

38−41. Same as 32−35 for the C III] emission complex. It is well known that C III]$\lambda\lambda$1909 is blended with Si III]$\lambda\lambda$1892 and to a lesser extent with Al III]$\lambda\lambda$1857. We do not attempt to deblend these lines. Therefore the redshift and red HWHM derived for this blend correspond to C III]$\lambda\lambda$1909. The blue HWHM is obviously affected by the blend.

42−43. Rest frame equivalent width and corresponding uncertainty in Å of the C III] emission complex.

44−47. Same as 32−35 for the Mg II emission line.

48−49. Rest frame equivalent width and corresponding uncertainty in Å of the Mg II emission line. We do not correct for the Fe II emission.

50. BAL flag from the visual inspection, `BAL_FLAG_VI`. If a BAL feature was identified in the course of the visual inspection, `BAL_FLAG_VI` is set to 1, 0 otherwise. Note that BAL quasars are flagged during the visual inspection at any redshift.

51−52. Balnicity index (BI; Weymann et al. 1991) for C IV troughs, and their errors, expressed in km s^{-1}. See definition in Sect. 5 of Pâris et al. (2012). The Balnicity index is measured for quasars with $z > 1.57$ only so that the trough enters into the BOSS wavelength region. If the BAL flag from the visual inspection is set to 1 and the BI is equal to 0, this means either that there is no C IV trough (but a trough is seen in another transition) or that the trough seen during the visual inspection does not meet the formal requirement of the BAL definition. In cases with bad fits to the continuum, the balnicity index and its error are set to −1.

53−54. Absorption index, and its error, for C IV troughs expressed in km s^{-1}. See definition in Sect. 5 of Pâris et al. (2012). In cases with bad continuum fit, the absorption index and its error are set to −1.

55. Following Trump et al. (2006), we calculate the reduced χ^2 which we call $\chi^2_{\rm trough}$ for each C IV trough from Eq. (3) in Pâris et al. (2012). We require that troughs have $\chi^2_{\rm trough} > 10$ to be considered as true troughs.

56. Number of C IV troughs of width larger than 2000 km s^{-1}.

57−58. Limits of the velocity range in which C IV troughs of width larger than 2000 km s^{-1} and reaching at least 10% below the continuum are to be found. Velocities are positive bluewards and the zero of the scale is at `Z_VI`. So if there are multiple troughs, this goes from one end of the first one to the other end of the last one.

59. Number of troughs of width larger than 450 km s^{-1}.

60−61. Same as 59−60 for C IV troughs of width larger than 450 km s^{-1}.

62−64. Rest frame equivalent width in Å of Si IV, C IV and Al III troughs detected in BAL quasars with BI > 500 km s^{-1} and SNR_1700 > 5. They are set to 0 otherwise or in cases where no trough is detected and to −1 if the continuum is not reliable.

65−66. The SDSS Imaging Run number and the Modified Julian Date (MJD) of the photometric observation used in the catalog.

67−70. Additional SDSS processing information: the photometric processing rerun number; the camera Cols. 1–6 containing the image of the object, the field number of the run containing the object, and the object identification number (see Stoughton et al. 2002, for descriptions of these parameters).

71−72. DR10 PSF fluxes, expressed in nanomaggies, and inverse variances (not corrected for Galactic extinction) in the five SDSS filters.

73−74. DR10 PSF AB magnitudes and errors (not corrected for Galactic extinction) in the five SDSS filters (Lupton et al. 1999).

75. DR8 PSF fluxes (not corrected for Galactic extinction), expressed in nanommagies, in the five SDSS filters. This photometry is the one that was used for the main quasar target selection (Ross et al. 2012).

76. The absolute magnitude in the i band at $z = 2$ calculated after correction for Galactic extinction and assuming $H_0 = 70$ km s^{-1} Mpc^{-1}, $\Omega_{\rm M} = 0.3$, $\Omega_\Lambda = 0.7$, and a power-law (frequency) continuum index of −0.5. The K-correction is computed using Table 4 from Richards et al. (2006). We use the SDSS primary photometry to compute this value.

77. The $\Delta(g - i)$ color, which is the difference in the Galactic extinction corrected $(g - i)$ for the quasar and that of the mean

of the quasars at that redshift. If $\Delta(g-i)$ is not defined for the quasar, which occurs for objects at either $z < 0.12$ or $z > 5.12$; the column will contain "−999.999".
78. Galactic extinction in the five SDSS bands based on the maps of Schlegel et al. (1998). The quasar target selection was done using these maps.
79. Galactic extinction in the five SDSS bands based on Schlafly & Finkbeiner (2011).
80. The logarithm of the Galactic neutral hydrogen column density along the line of sight to the quasar. These values were estimated via interpolation of the 21-cm data from Stark et al. (1992), using the COLDEN software provided by the *Chandra* X-ray Center. Errors associated with the interpolation are expected to be typically less than $\approx 1 \times 10^{20}$ cm^{-2} (e.g., see Sect. 5 of Elvis et al. 1994).
81. The logarithm of the vignetting-corrected count rate (photons s^{-1}) in the broad energy band (0.1–2.4 keV) from the ROSAT All-Sky Survey Faint Source Catalog (Voges et al. 2000) and the ROSAT All-Sky Survey Bright Source Catalog (Voges et al. 1999). The matching radius was set to 30″ (see Sect. 4.5.6).
82. The S/N of the ROSAT measurement.
83. Angular separation between the SDSS and *ROSAT* All-Sky Survey locations (in arcseconds).
84. Number of *XMM-Newton* matches in a 5″ radius around the SDSS-DR10 quasar positions.
85. Soft X-ray flux (0.5–2 keV) from *XMM-Newton* matching, expressed in erg cm^{-2} s^{-1}. In case of several observations, the one with the longest exposure time is used to compute the flux.
86. Hard X-ray flux (2–12 keV) from *XMM-Newton* matching, expressed in erg cm^{-2} s^{-1}.
87. X-ray luminosity in the 0.5–2 keV band of *XMM-Newton*, expressed in erg s^{-1}. This value is computed using the visual inspection redshift (Z_VI) and $H_0 = 70$ km s^{-1} Mpc^{-1}, $\Omega_m = 0.3$, $\Omega_\Lambda = 0.7$.
88. X-ray luminosity in the 2–12 keV band of *XMM-Newton*, expressed in erg s^{-1}. This value is computed using the visual inspection redshift (Z_VI) and $H_0 = 70$ km s^{-1} Mpc^{-1}, $\Omega_m = 0.3$, $\Omega_\Lambda = 0.7$.
89. In case of unreliable or no detection in the 2–10 keV band the flux reported in column #86 is an upper limit. In that case, the LUMX2_10_UPPER flag listed in this column is set to −1.
90. Angular separation between the *XMM-Newton* and SDSS-DR10 locations, expressed in arcsec.
91. If a SDSS-DR10 quasar matches with GALEX photometring, GALEX_MATCHED is set to 1, 0 if not.
92–95. UV fluxes and inverse variances from GALEX, aperture-photometered from the original GALEX images in the two bands FUV and NUV. The fluxes are expressed in nanomaggies.
96–97. The *J* magnitude and error from the Two Micron All Sky Survey All-Sky Data Release Point Source Catalog (Cutri et al. 2003) using a matching radius of 2.0″ (see Sect. 4.5.3). A non-detection by 2MASS is indicated by a "0.000" in these columns. Note that the 2MASS measurements are Vega-based, not AB, magnitudes.
98–99. S/N in the *J* band and corresponding 2MASS jr_d flag that gives the meaning of the peculiar values of the magnitude and its error[9].
100–103. Same as 96–99 for the *H*-band.
104–107. Same as 96–99 for the *K*-band.
108. Angular separation between the SDSS and 2MASS positions (in arcseconds).
109–110. The *w*1 magnitude and error from the Wide-field Infrared Survey Explorer (WISE; Wright et al. 2010) All-Sky Data Release Point Source Catalog using a matching radius of 2″.
111–112. S/N and χ^2 in the WISE *w*1 band.
113–116. Same as 109–112 for the *w*2-band.
117–120. Same as 109–112 for the *w*3-band.
121–124. Same as 109–112 for the *w*4-band.
125. WISE contamination and confusion flag.
126. Angular separation between SDSS and WISE positions (in arcsec).
127. If a SDSS-DR10 quasar matches UKIDSS aperture-photometering data, UKIDSS_MATCHED is set to 1, it is set to 0 if not.
128–135. Flux and error from UKIDSS, aperture-photometered from the original UKIDSS images in the four bands *Y*, *J*, *H* and *K*. The fluxes and errors are expressed in W m^{-2} Hz^{-1}.
136. If there is a source in the FIRST radio catalog (version February 2012) within 2.0″ of the quasar position, the FIRST_MATCHED flag provided in this column is set to 1, O if not. If the quasar lies outside of the FIRST footprint, it is set to −1.
137. This column contains the FIRST peak flux density, expressed in mJy.
138. The S/N of the FIRST source whose flux is given in Col. 136.
139. Angular separation between the SDSS and FIRST positions (in arcsec).

[9] see http://www.ipac.caltech.edu/2mass/releases/allsky/doc/explsup.html

6. Conclusions

We have presented the second quasar catalog of the SDSS-III/BOSS survey based on the first three years of observations. It contains 166 583 quasars, 117 668 having $z > 2.15$, with robust identification from visual inspection and refined redshift measurements based on the results of a principal component analysis of the spectra. The present catalog is almost twice as large as the catalog of the previous release (DR9Q; Pâris et al. 2012) As part of the DR10Q catalog, we also release a catalog of 16 461 BAL quasars and their properties together with a multi-wavelength matching with GALEX, 2MASS, UKIDSS, WISE, FIRST, RASS, and XMM observations.

The next SDSS public release, SDSS-DR12, is scheduled for December 2014 and will contain more than 250 000 quasars, including about 200 000 $z > 2.15$ quasars.

Acknowledgements. I.P. received partial support from Center of Excellence in Astrophysics and Associated Technologies (PFB 06). The French Participation Group to SDSS-III was supported by the Agence Nationale de la Recherche under contracts ANR-08-BLAN-0222 and ANR-12-BS05-0015. A.D.M. is a research fellow of the Alexander von Humboldt Foundation of Germany and was partially supported through NSF Grant 1211112 and NASA ADAP award NNX12AE38G. Funding for SDSS-III has been provided by the Alfred P. Sloan Foundation, the Participating Institutions, the National Science Foundation, and the US Department of Energy Office of Science. The SDSS-III web site is http://www.sdss3.org/. SDSS-III is managed by the Astrophysical Research Consortium for the Participating Institutions of the SDSS-III Collaboration including the University of Arizona, the Brazilian Participation Group, Brookhaven National Laboratory, Carnegie Mellon University, University of Florida, the French Participation Group, the German Participation Group, Harvard University, the Instituto de Astrofisica de Canarias, the Michigan State/Notre Dame/JINA Participation Group, Johns Hopkins University, Lawrence Berkeley National Laboratory, Max Planck Institute for Astrophysics, Max Planck Institute for Extraterrestrial Physics, New Mexico State University, New York University, Ohio State University, Pennsylvania State University, University of Portsmouth, Princeton University, the Spanish Participation Group, University of Tokyo, University of Utah,

Vanderbilt University, University of Virginia, University of Washington, and Yale University.

Appendix A: List of target selection flags

Table A.1 presents the list of target selection bits used to select the parent sample of quasar targets (i.e., without serendipitous quasars from galaxy targets) together with the result of the visual inspection.

The main quasar target selection (Ross et al. 2012) is encoded with the target selection flag `BOSS_TARGET1` while the various ancillary program target selections are encoded via the flags `ANCILLARY_TARGET1` and `ANCILLARY_TARGET2` (Dawson et al. 2013). A given quasar target can be selected by various algorithms or different ancillary programs, and hence the numbers given in Table A.1 are not cumulative.

Table A.1. Number of visually inspected DR10 BOSS quasar targets (third column) and identifications in the DR10Q catalog for each target selection method (first column; see Table 4 of Ross et al. 2012, and Tables 6 and 7 in the appendix of Dawson et al. 2013). These categories overlap because many objects are selected by multiple algorithms.

Selection	Maskbits	# Objects	# QSO	# QSO $z > 2.15$	# STAR	# GALAXY	# ?	# BAD
BOSS_TARGET1								
QSO_CORE	10	3402	1349	1089	1941	64	40	8
QSO_BONUS	11	4149	788	469	3231	84	35	11
QSO_KNOWN_MIDZ	12	15 020	14 919	14 781	34	1	40	26
QSO_KNOWN_LOHIZ	13	57	57	1	0	0	0	0
QSO_NN	14	139 310	92 311	74 711	44 192	1119	781	907
QSO_UKIDSS	15	48	27	22	19	2	0	0
QSO_LIKE_COADD	16	1368	314	229	918	55	61	20
QSO_LIKE	17	109 433	66 565	46 193	38 749	2023	1127	969
QSO_FIRST_BOSS	18	6195	4884	3314	638	240	359	74
QSO_KDE	19	162 988	94 868	73 075	64 277	1680	1115	1048
QSO_CORE_MAIN	40	130 024	82 672	67 642	43 885	1374	1051	1042
QSO_BONUS_MAIN	41	264 278	144 539	108 756	108 993	5473	2812	2461
QSO_CORE_ED	42	32 659	21 863	18 553	9930	269	285	312
QSO_CORE_LIKE	43	34 919	25 924	18 945	8003	446	266	280
QSO_KNOWN_SUPPZ	44	57	57	1	0	0	0	0
ANCILLARY_TARGET1								
BLAZGVAR	6	2	1	0	0	0	1	0
BLAZR	7	6	2	0	0	4	0	0
BLAZXR	8	361	102	5	27	202	30	0
BLAZXRSAL	9	3	3	1	0	0	0	0
BLAZXRVAR	10	1	0	0	0	0	1	0
XMMBRIGHT	11	413	314	15	14	84	1	0
XMMGRIZ	12	62	14	8	21	18	8	1
XMMHR	13	476	141	14	24	294	14	3
XMMRED	14	337	57	2	42	234	1	3
FBQSBAL	15	6	5	2	0	0	1	0
LBQSBAL	16	6	6	0	0	0	0	0
ODDBAL	17	21	15	6	1	1	4	0
OTBAL	18	11	2	0	0	0	9	0
PREVBAL	19	10	10	2	0	0	0	0
VARBAL	20	1007	999	370	0	0	4	4
QSO_AAL	22	324	319	2	1	1	1	2
QSO_AALS	23	622	617	35	0	0	1	4
QSO_IAL	24	195	194	2	0	0	1	0
QSO_RADIO	25	157	155	8	1	0	1	0
QSO_RADIO_AAL	26	104	104	0	0	0	0	0
QSO_RADIO_IAL	27	56	55	0	0	0	1	0
QSO_NOAALS	28	53	53	1	0	0	0	0
QSO_GRI	29	1503	584	561	466	300	114	39
QSO_HIZ	30	393	0	0	351	3	15	24
QSO_RIZ	31	1089	70	66	838	111	50	20
BLAZGRFLAT	50	74	42	6	9	5	15	3
BLAZGRQSO	51	94	58	14	14	3	19	0
BLAZGX	52	8	2	0	5	1	0	0
BLAZGXQSO	53	31	29	2	0	1	1	0
BLAZGXR	54	100	33	3	12	21	34	0
CXOBRIGHT	58	99	66	2	3	27	3	0
CXORED	59	17	6	2	3	4	3	1
ANCILLARY_TARGET2								
HIZQSO82	0	57	2	2	54	1	0	0
HIZQSOIR	1	86	2	1	77	0	4	3
KQSO_BOSS	2	183	86	40	88	4	4	1
QSO_VAR	3	1370	865	311	424	79	0	2
QSO_VAR_FPG	4	579	557	284	5	3	9	5
RADIO_2LOBE_QSO	5	806	402	39	265	76	48	15
QSO_SUPPZ	7	2824	2805	14	2	0	4	13
QSO_VAR_SDSS	8	15 375	5857	3003	8329	224	551	414
QSO_WISE_SUPP	9	5007	2988	999	1561	303	135	20

Table B.1. Description of the file that contains the superset from which we derive the DR10Q catalog.

Column	Name	Format	Description
1	SDSS_NAME	STRING	SDSS-DR10 designation hhmmss.ss+ddmmss.s (J2000)
2	RA	DOUBLE	Right Ascension in decimal degrees (J2000)
3	DEC	DOUBLE	Declination in decimal degrees (J2000)
4	THING_ID	INT32	Thing_ID
5	PLATE	INT32	Spectroscopic Plate number
6	MJD	INT32	Spectroscopic MJD
7	FIBERID	INT32	Spectroscopic Fiber number
8	Z_VI	DOUBLE	Redshift from visual inspection
9	Z_PIPE	DOUBLE	Redshift from BOSS pipeline
10	ERR_ZPIPE	DOUBLE	Error on BOSS pipeline redshift
11	ZWARNING	INT32	ZWARNING flag
12	CLASS_PERSON	INT32	Classification from the visual inspection
13	Z_CONF_PERSON	INT32	Redshift confidence from visual inspection
14	SDSS_MORPHO	INT32	SDSS morphology flag 0 = point source 1 = extended
15	BOSS_TARGET1	INT64	BOSS target flag for main survey
16	ANCILLARY_TARGET1	INT64	BOSS target flag for ancillary programs
17	ANCILLARY_TARGET2	INT64	BOSS target flag for ancillary programs
18	PSFFLUX	FLOAT[5]	Flux in the u, g, r, i and z-bands (not corrected for Galactic extinction)
19	IVAR_PSFLUX	FLOAT[5]	Inverse variance of u, g, r, i and z fluxes
20	PSFMAG	FLOAT[5]	PSF magnitudes in u, g, r, i and z-bands (not corrected for Galactic extinction)
21	ERR_PSFMAG	FLOAT[5]	Error in u, g, r, i and z PSF magnitudes
22	TARGET_FLUX	FLOAT[5]	TARGET flux in the u, g, r, i and z-bands (not corrected for Galactic extinction)
23	GAL_EXT	FLOAT[5]	Galactic extinction in the 5 SDSS bands (from Schlegel et al. 1998)

Notes. This file contains the result from the visual inspection as described in Table 2.

Appendix B: Description of the superset of DR10Q

We visually inspected 321 729 quasar candidates to produce the DR10Q catalog. We provide the basic properties (spectroscopic and photometric) of all the quasar targets, together with the result of the visual inspection, in the form of the binary fits file that is available at the SDSS public website[10]. The FITS header contains all of the required documentation (format, name, unit of each column).

References

Ahn, C. P., Alexandroff, R., Allende Prieto, C., et al. 2012, ApJS, 203, 21
Ahn, C. P., Alexandroff, R., Allende Prieto, C., et al. 2013, ApJS, submitted [arXiv:1307.7735]
Aihara, H., Allende Prieto, C., An, D., et al. 2011, ApJS, 193, 29
Alexandroff, R., Strauss, M. A., Greene, J. E., et al. 2013, MNRAS, 435, 3306
Allen, J. T., Hewett, P. C., Maddox, N., Richards, G. T., & Belokurov, V. 2011, MNRAS, 410, 860
Anderson, L., Aubourg, E., Bailey, S., et al. 2012, MNRAS, 427, 3435
Becker, R. H., White, R. L., & Helfand, D. J. 1995, ApJ, 450, 559
Bolton, A. S., Schlegel, D. J., Aubourg, É., et al. 2012, AJ, 144, 144
Bovy, J., Hennawi, J. F., Hogg, D. W., et al. 2011, ApJ, 729, 141
Bovy, J., Myers, A. D., Hennawi, J. F., et al. 2012, ApJ, 749, 41
Busca, N. G., Delubac, T., Rich, J., et al. 2013, A&A, 552, A96
Croom, S. M., Shanks, T., Boyle, B. J., et al. 2001, MNRAS, 325, 483
Croom, S. M., Smith, R. J., Boyle, B. J., et al. 2004, MNRAS, 349, 1397
Croom, S. M., Richards, F. T., Shanks, T., & et al. 2009, MNRAS, 392, 19
Cutri, R. M., Skrutskie, M. F., van Dyk, S., et al. 2003, VizieR Online Data Catalog: II/246
Dawson, K. S., Schlegel, D. J., Ahn, C. P., et al. 2013, AJ, 145, 10
Eisenstein, D. J., Weinberg, D. H., Agol, E., et al. 2011, AJ, 142, 72
Elvis, M., Lockman, F. J., & Fassnacht, C. 1994, ApJS, 95, 413
Fukugita, M., Ichikawa, T., Gunn, J. E., et al. 1996, AJ, 111, 1748
Gibson, R. R., Jiang, L., Brandt, W. N., et al. 2009, ApJ, 692, 758
Gunn, J. E., Carr, M., Rockosi, C., et al. 1998, AJ, 116, 3040
Gunn, J. E., Siegmund, W. A., Mannery, E. J., et al. 2006, AJ, 131, 2332
Hall, P. B., Anderson, S. F., Strauss, M. A., et al. 2002, ApJS, 141, 267
Hogg, D. W., Finkbeiner, D. P., Schlegel, D. J., & Gunn, J. E. 2001, AJ, 122, 2129
Ivezić, Ž., Lupton, R. H., Schlegel, D., et al. 2004, Astron. Nachr., 325, 583
Kirkpatrick, J. A., Schlegel, D. J., Ross, N. P., et al. 2011, ApJ, 743, 125
Krawczyk, C. M., Richards, G. T., Mehta, S. S., et al. 2013, ApJS, 206, 4
Lawrence, A., Warren, S. J., Almaini, O., et al. 2007, MNRAS, 379, 1599
Lupton, R., Gunn, J. E., Ivezić, Z., et al. 2001, in Astronomical Data Analysis Software and Systems X, eds. F. R. Harnden Jr., F. A. Primini, & H. E. Payne, ASP Conf. Ser., 238, 269
Lupton, R. H., Gunn, J. E., & Szalay, A. S. 1999, AJ, 118, 1406
Martin, D. C., Fanson, J., Schiminovich, D., et al. 2005, ApJ, 619, L1
McDonald, P., & Eisenstein, D. J. 2007, Phys. Rev. D, 76, 063009
Padmanabhan, N., Schlegel, D. J., Finkbeiner, D. P., et al. 2008, ApJ, 674, 1217
Pâris, I., Petitjean, P., Rollinde, E., et al. 2011, A&A, 530, A50
Pâris, I., Petitjean, P., Aubourg, É., et al. 2012, A&A, 548, A66
Pier, J. R., Munn, J. A., Hindsley, R. B., et al. 2003, AJ, 125, 1559
Richards, G. T., Nichol, R. C., Gray, A. G., et al. 2004, ApJS, 155, 257
Richards, G. T., Strauss, M. A., Fan, X., et al. 2006, AJ, 131, 2766
Richards, G. T., Myers, A. D., Gray, A. G., et al. 2009, ApJS, 180, 67
Ross, N. P., Myers, A. D., Sheldon, E. S., et al. 2012, ApJS, 199, 3
Schlafly, E. F., & Finkbeiner, D. P. 2011, ApJ, 737, 103
Schlegel, D. J., Finkbeiner, D. P., & Davis, M. 1998, ApJ, 500, 525
Schmidt, M. 1963, Nature, 197, 1040
Schneider, D. P., Richards, G. T., Hall, P. B., et al. 2010, AJ, 139, 2360
Skrutskie, M. F., Cutri, R. M., Stiening, R., et al. 2006, AJ, 131, 1163
Slosar, A., Iršič, V., Kirkby, D., et al. 2013, J. Cosmol. Astropart. Phys., 4, 26
Smee, S. A., Gunn, J. E., Uomoto, A., et al. 2013, AJ, 146, 32
Smith, J. A., Tucker, D. L., Kent, S., et al. 2002, AJ, 123, 2121
Spergel, D. N., Verde, L., Peiris, H. V., et al. 2003, ApJS, 148, 175
Stark, A. A., Gammie, C. F., Wilson, R. W., et al. 1992, ApJS, 79, 77
Stoughton, C., Lupton, R. H., Bernardi, M., et al. 2002, AJ, 123, 485
Trump, J. R., Hall, P. B., Reichard, T. A., et al. 2006, ApJS, 165, 1
Tucker, D. L., Kent, S., Richmond, M. W., et al. 2006, Astron. Nachr., 327, 821
Voges, W., Aschenbach, B., Boller, T., et al. 1999, A&A, 349, 389
Voges, W., Aschenbach, B., Boller, T., et al. 2000, IAU Circ., 7432, 3
Watson, M. G., Schröder, A. C., Fyfe, D., et al. 2009, A&A, 493, 339
Weymann, R. J., Morris, S. L., Foltz, C. B., & Hewett, P. C. 1991, ApJ, 373, 23
White, M., Myers, A. D., Ross, N. P., et al. 2012, MNRAS, 424, 933
Wright, E. L., Eisenhardt, P. R. M., Mainzer, A. K., et al. 2010, AJ, 140, 1868
Yèche, C., Petitjean, P., Rich, J., et al. 2010, A&A, 523, A14
York, D. G., Adelman, J., Anderson, Jr., J. E., et al. 2000, AJ, 120, 1579

[10] http://www.sdss3.org/dr10/algorithms/qso_catalog.php

[1] Departamento de Astronomía, Universidad de Chile, 36-D Casilla, Santiago, Chile
e-mail: paris@iap.fr

[2] UPMC-CNRS, UMR 7095, Institut d'Astrophysique de Paris, 75014 Paris, France
[3] APC, Astroparticule et Cosmologie, Uniiversité Paris Diderot, CNRS/IN2P3, CEA/Irfu, Observatoire de Paris, Sorbonne Paris Cité, 10 rue Alice Domon & Léonie Duquet, 75205 Paris Cedex 13, France
[4] Lawrence Berkeley National Laboratory, 1 Cyclotron Road, Berkeley CA 94720, USA
[5] Department of Physics and Astronomy, University of Wyoming, Laramie WY 82071, USA
[6] Max-Planck-Institut für Astronomie, Königstuhl 17, 69117 Heidelberg, Germany
[7] Instituto de Astrofisica de Canarias (IAC), 38200 La Laguna, Tenerife, Spain
[8] Universidad de La Laguna (ULL), Dept. Astrofisica, 38206 La Laguna, Tenerife, Spain
[9] Department of Physics and Astronomy, York University, Toronto, ON M3J1P3, Canada
[10] Princeton University Observatory, Peyton Hall, Princeton NJ 08544, USA
[11] University of Washington, Dept. of Astronomy, Box 351580, Seattle WA 98195, USA
[12] Apache Point Observatory, PO Box 59, Sunspot NM 88349-0059, USA
[13] CEA, Centre de Saclay, Irfu/SPP, 91191, Gif-sur-Yvette, France
[14] Institute for Advanced Study, Einstein Drive, Princeton NJ 08540, USA
[15] Department of Astronomy and Astrophysics, The Pennsylvania State University, University Park, PA 16802, USA
[16] Institute for Gravitation and the Cosmos, The Pennsylvania State University, University Park, PA 16802, USA
[17] Department of Physics and Astronomy, University of Utah, 115 S 1400 E, Salt Lake City, UT 84112, USA
[18] Steward Observatory, University of Arizona, 933 North Cherry Avenue, Tucson AZ 85721, USA
[19] Faculty of Sciences, Department of Astronomy and Space Sciences, Erciyes University, 38039 Kayseri, Turkey
[20] Institute of Theoretical Physics, University of Zurich, Winterthurerstrasse 190, 8057 Zurich, Switzerland
[21] Department of Astronomy, University of Florida, Gainesville FL 32611-2055, USA
[22] Institute of Astronomy, University of Cambridge, Madingley Road, Cambridge CB3 0HA, UK
[23] McWilliams Center for Cosmology, Department of Physics, Carnegie Mellon University, Pittsburgh PA 15213, USA
[24] Institució Catalana de Recerca i Estudis Avançats, Barcelona, Catalonia
[25] Institut de Ciències del Cosmos, Universitat de Barcelona (UB-IEEC), Barcelona, Catalonia
[26] Department of Astronomy, Ohio State University, Columbus OH 43210, USA
[27] Institute of Cosmology and Gravitation, University of Portsmouth, Dennis Sciama building, Portsmouth P01 3FX, UK
[28] Instituto de Física, UFRGS, Caixa Postal 15051, RS - 91501-970 Porto Alegre, Brazil
[29] Laboratório Interinstitucional de e-Astronomia, - LIneA, Rua Gal. José Cristino 77, RJ - 20921-400 Rio de Janeiro, Brazil
[30] INAF–Osservatorio Astronomico di Trieste, via G. B. Tiepolo 11, 34131 Trieste, Italy
[31] INFN/National Institute for Nuclear Physics, via Valerio 2, 34127 Trieste, Italy
[32] Center for Cosmology and Particle Physics, New York University, New York NY 10003, USA
[33] PITT PACC, Department of Physics and Astronomy, University of Pittsburgh, Pittsburgh PA 15260, USA
[34] Department of Astronomy and Astrophysics, University of Chicago, 5640 South Ellis Avenue, Chicago IL 60637, USA
[35] Enrico Fermi Institute, University of Chicago, 5640 South Ellis Avenue, Chicago IL 60637, USA